In Situ Observations of Cirrus Cloud Microphysical Properties Using the Counterflow Virtual Impactor

K. B. NOONE,* K. J. NOONE,* J. HEINTZENBERG, J. STRÖM, AND J. A. OGREN†

Department of Meteorology, Stockholm University, Arrhenius Laboratory, Stockholm, Sweden

(Manuscript received 22 November 1991, in final form 19 August 1992)

ABSTRACT

This study presents a new technique for making in situ measurements of cirrus cloud microphysical properties. Sampling of cirrus clouds was performed using a counterflow virtual impactor (CVI). The CVI was used to sample cloud elements larger than 4 μm in aerodynamic diameter. In conjunction with a Lyman-α hygrometer, this gave a direct measurement of the condensed water content. Sampling the cloud elements with the CVI also allowed the authors to examine the size distribution of the residual particles produced by evaporation of the cloud elements. This study discusses and evaluates the CVI technique for use in sampling cirrus clouds, especially for sampling small cloud elements. Measurements of condensed water content and cloud-element (crystal and droplet) concentrations for cirrus uncinus, floccus, and cirrostratus clouds made using the CVI during the International Cirrus Experiment experiment are presented. Examples of size distributions of the residual aerosol particles from cirrus cloud elements are also presented.

1. Introduction

There is no doubt that cirrus clouds are important for the radiation balance of the earth, but it is still unknown if the feedback of cirrus clouds on the greenhouse effect is positive or negative (Stephens et al. 1990). Stephens et al. consider this to be because the dynamics, microphysics, and radiative properties of cirrus clouds are still not known with sufficient accuracy. Increasingly, attention is also being given to the topic of small crystals in cirrus clouds. Heymsfield and Platt (1984) estimated that 35%–50% of the total visible extinction in cirrus clouds can be attributed to particles in the 2–20-μm-diameter range. Very few measurements have been made of these small crystals. Measurements made in cirrus clouds with slides or replicators have been made on a few occasions (e.g., Heymsfield and Knollenberg 1972; Heymsfield 1975), but the sampling volumes are too small to give statistically representative data on number concentration and condensed water content. These measurements were primarily used to determine the crystal habits. The PMS forward-scattering spectrometer probe (FSSP) has also been used (e.g., Heymsfield 1977; Heymsfield and Platt 1984). It does not count and size ice crystals correctly (Gardiner and Hallett 1985), and therefore, it can give only an indication that small crystals are present in the cloud. Apparently, the sizing problems in cirrus clouds with the FSSP were encountered most often in the presence of large crystals. The FSSP may be more accurate when only smaller crystals are present, though some artifacts have been observed in warm cirrus clouds (Heymsfield and Miloshevich 1989). The instruments most often used in the study of microphysics in cirrus clouds are the PMS 1D and 2D probes (e.g., Heymsfield and Knollenberg 1972; Heymsfield 1975, 1977, 1986; Heymsfield et al. 1990; Sassen et al. 1989). These instruments do not sense crystals smaller than 50–100 μm. Another drawback is that the probes do not give a direct measurement of the condensed water content. Assumptions about the three-dimensional structure and the orientation of the cloud elements have to be made before the condensed water content can be estimated.

In the autumn of 1989, the International Cirrus Experiment (ICE '89) was conducted over the North Sea. It was an experiment designed to study the microphysics, dynamics, and radiative characteristics of cirrus clouds as a contribution to the International Satellite Cloud Climatology Project (ISCCP). In this experiment, the counterflow virtual impactor (CVI, Ogren et al. 1985) was employed for the first time in high-altitude clouds. In part, this experiment was to evaluate the CVI technique for sampling small cirrus

* Current affiliation: Center for Atmospheric Chemistry Studies, Graduate School of Oceanography, University of Rhode Island, Narragansett, Rhode Island.

† Current affiliation: NOAA CMDL R/E/CG, 325 Broadway, Boulder, Colorado.

Corresponding author address: Dr. K. Birgitta Noone, University of Rhode Island, Center for Atmospheric Chemistry Studies, Graduate School of Oceanography, Narragansett, RI 02882-1197.

cloud elements. With the CVI, we were able to obtain a direct measurement of the condensed water content in cirrus clouds. Since the CVI samples crystals and droplets with an aerodynamic diameter down to approximately 4 μm, the measurements also included the small cloud elements.

With the CVI, we were also able to study the number and size distribution of the residual particles left behind when the crystals (or droplets) were evaporated in the probe. Although it is not within the scope of this paper to discuss the implications of the measured residual particles on cirrus cloud formation or the life cycles of cirrus crystals, a few examples of the size distributions will be shown.

2. Experimental description

The CVI is an instrument that has been used in a number of experiments to study the microphysics and chemistry of clouds (e.g., Ogren et al. 1988; Noone et al. 1988b; Twohy et al. 1989; Heintzenberg et al. 1989; Noone et al. 1992). During ICE in September and October 1989, the CVI was used for the first time to collect ice crystals in cirrus clouds. A detailed description of how the CVI works has been given by Ogren et al. (1985) and Noone et al. (1988a). A brief description of the CVI will be given here, emphasizing modifications in the system for sampling at cirrus altitudes.

a. *Counterflow virtual impactor*

The CVI is a device that inertially separates large particles (droplets, ice crystals) in an airstream from smaller particles and surrounding gases. For purposes of simplicity, and because we will be discussing sampling of clouds, we shall refer to large "particles" as *cloud elements.* In cirrus clouds, these cloud elements are, in most cases, ice crystals. A schematic diagram of the CVI probe tip is shown in Fig. 1. The tip consists of two concentric tubes joined at the leading edge. The outer tube is solid stainless steel, as is the aft portion of the inner tube. The first few centimeters of the inner tube are porous stainless steel. Warm, dry, particle-free air is pumped through the annular region between the tubes out toward the tip. This is called the *supply flow* (F_1 in Fig. 1). Because the two tubes are joined, this "carrier air" is forced radially inward through the porous tube. Some fraction of the supply flow is pulled back toward the sampling instrumentation in the interior tube. This is called the *sample flow* (F_2 in Fig. 1). The sample and supply flow rates are adjustable; if the supply flow rate is greater than the sample flow rate, the result is a flow of carrier air out the tip of the probe. This is called the *excess,* or *counter flow* (F_3 in Fig. 1), thus the name counterflow virtual impactor. At some point within the confines of the porous tubing, there is a region (theoretically a plane) where the net velocity is zero. This is called the stagnation plane.

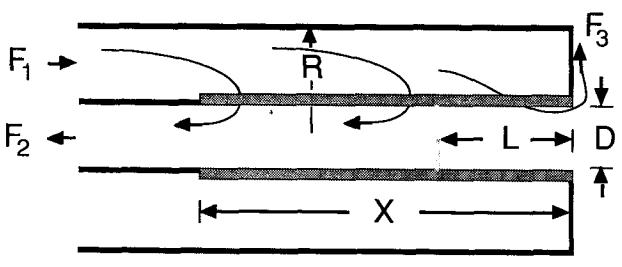

FIG. 1. The CVI probe tip. Here F_1 is the return airflow, F_2 is the sample airflow, F_3 is the excess airflow, R is the probe radius (4 mm), D is the inlet diameter (3 mm), X is the length of the porous tube (25 mm), and L is the distance to the stagnation plane (variable). The dimensions are for the probe used in the ICE '89 experiment. When flown, the cloud elements would have approached the probe (depicted in the diagram) from the right.

When flown on an aircraft, trajectories of cloud elements that are sufficiently large can cross the streamlines of air flowing around the probe, causing the cloud elements to impact upon the probe. The minimum cloud element size that impacts on the probe can be calculated using the Stoke's number. The probe flown in the ICE '89 experiment had an outer diameter of 8 mm. The velocity of the aircraft was typically 200 m s^{-1}, giving a minimum cut size of approximately 4 μm in diameter (Noone et al. 1988a). The cut size is an aerodynamic diameter; nonspherical cloud elements with aerodynamic diameters larger than 4 μm were sampled, regardless of their exact shape.

To be sampled, cloud elements must first impact on the inlet of the probe. They must also have sufficient inertia (a sufficiently long stopping distance) to go through the region of outwardly moving air past the stagnation plane. Cloud elements whose stopping distance is shorter than the distance from the probe tip to the stagnation plane will be forced back out the tip of the probe, and not be sampled. Being volatile, the cloud elements will begin to evaporate as soon as they have passed the entrance of the probe. Because of the difference in the time scales for evaporation and deceleration, the size of the droplet or crystal will not change sufficiently to influence its stopping distance.

Once entrained in the sample stream, the cloud elements continue to evaporate. The condensed water associated with the cloud elements is driven into the gas phase, as are any dissolved gases or volatile material dissolved in them. The nonvolatile or insoluble material in the cloud elements remains behind as a *residual particle.* It is important to distinguished between *residual* and *interstitial* particles. Residual particles are those particles left behind when the cloud elements are evaporated in the CVI. Interstitial particles are small particles present in the ambient air. These are not sampled by the CVI.

The ambient sampling rate of the CVI is given by the product of the velocity of the air flowing past the probe tip and the cross-sectional area of the inlet. For this experiment, the ambient sampling rate was 85 l

min^{-1}. Cloud elements removed from the ambient airstream were embedded in a flow of typically 5 l min^{-1}. As a result, all of the measured quantities (water vapor that was formerly condensed water, residual particles from the cloud elements) were concentrated (enriched) by a factor of approximately 17. The enrichment factor varied between roughly 10 and 40 during the course of the experiment, depending upon the sample flow rate.

The CVI probe was mounted on the top centerline of the aircraft, on the second top port. The first port was unused, so there were no obstructions upstream of the probe.

b. Instrumentation

A schematic diagram of the sampling train used in conjunction with the CVI is shown in Fig. 2. The sample stream was conducted through approximately 2 m of 0.5-in. outer-diameter nylon tubing to a stainless steel sample plenum. Here the sample flow was split to the various instruments. For the experiment described here, these were a TSI 3760 condensation nucleus counter (CNC; TSI Inc., St. Paul, Minnesota), a PMS ASASP-X-SP optical particle counter (OPC; PMS, Boulder, Colorado), and two Lyman-α hygrometers that were constructed at Stockholm University.

1) HYGROMETER

The hygrometers used in this experiment are dual-beam Lyman-α hygrometers (Zuber and Witt 1987; Zuber 1989). The instruments use a common lamp and two detectors, one for reference air and one for sample air. This configuration removes the effects of fluctuations in the lamp intensity. To increase the dynamic range of the condensed water content measurements, two hygrometers were used in parallel. One had an absorption pathlength of 5 cm (Lyman 1), and the other had a pathlength of 15 cm (Lyman 2). The hygrometers were first zeroed by drawing dry reference air from a common source through the sample and reference chambers. This procedure allowed for determination of electronic drift in the detectors. Once any electronic drift was removed, the water content of the CVI carrier air was measured. This allowed us to determine a detection limit for subsequent condensed water content measurements. The CVI and the hygrometers had separate driers in this experiment. Both used a type-5 molecular sieve as desiccant. This procedure was carried out before and (usually) after each flight. With frequent zeroing, the detection limit of the hygrometers can be reduced to 0.1 mg m^{-3} (Zuber and Witt 1987).

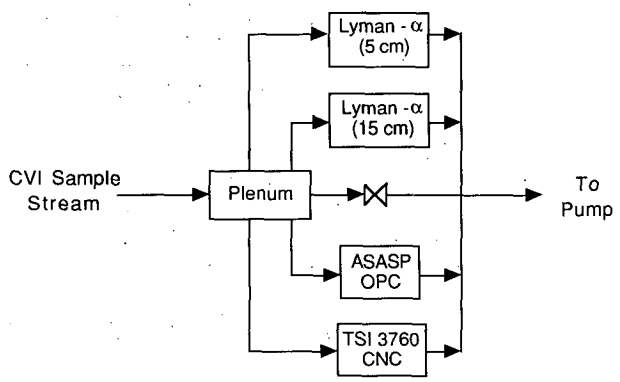

FIG. 2. CVI sample flow diagram. The plenum was situated roughly 2 m downstream of the CVI tip.

Although the detection limit of the hygrometers was 0.1 mg m^{-3}, this does not represent the detection limit of the entire CVI system. The background water vapor concentration of the dry carrier air in the CVI was higher than the dry reference air used in the hygrometers. The water vapor content of the CVI carrier was determined with the hygrometers on six occasions. On average, the water vapor concentration was determined by both hygrometers to be 25 mg m^{-3} in the CVI. The standard deviation for Lyman 1 was 8 mg m^{-3}, and 7 mg m^{-3} for Lyman 2. The reported condensed water content (CWC) values have been corrected for this average carrier air background. The CWC detection limit for the CVI system as a whole will be taken as this average carrier air background plus twice the largest of the two hygrometer standard deviations, 41 mg m^{-3}. This value refers to the water concentration measured in the CVI sample stream. In terms of ambient concentrations, the detection limit would be 2 mg m^{-3} (due to the enrichment effect of the CVI). The accuracy of the Lyman-α hygrometers was determined prior to the experiment by comparisons with an Assman psychrometer while sampling ambient air. Agreement with the psychrometer was better than 10%.

2) CONDENSATION NUCLEUS COUNTER

The concentration of the residual particles was determined using a TSI 3760 CNC. Assuming that upon evaporation a single cloud element yields a single aerosol particle, the residual particle number concentration corresponds to the number concentration of cloud elements larger than the cut size of the CVI. This assumption has been tested for land-based CVI systems sampling in warm clouds (i.e., Ogren et al. 1992), although no specific tests have been performed for the aircraft CVI probe. The CNC used senses particles larger than 0.02 μm in diameter. The counting error in the concentration measurement of the CNC is given by $\sqrt{N}/N$, where N is the number of particles counted by the instrument in the given averaging interval. For the 30-s averaging interval reported in this experiment, the counting error for the 3760 instrument was 5% at a particle concentration of 600 l^{-1}. In some of the flights, problems were encountered with the CNC. During rapid decreases in pressure, spurious particle

counts were observed. This was due to liquid butanol bubbling into the saturation chamber of the instrument. These events could easily be distinguished from real cloud events due to the extremely high number counts and the shape of the peak produced when plotted as a time series. The TSI 3760 has previously been calibrated for use at low pressures (Noone et al. 1990).

3) OPTICAL PARTICLE COUNTER

The residual particle size distributions were measured with a PMS ASASP-X-SP optical particle counter. PMS also manufactures an instrument (formerly the ASASP-100X, now the PCASP-100X) that can be externally mounted on an aircraft and that sizes particles between 0.1 and 3 μm. The ASASP-100X was *not* the instrument we used in this experiment. The ASASP-X-SP is an instrument more commonly used in aerosol laboratories or on the ground. This instrument has a nominal size range of 0.1–10 μm in diameter over 32 channels. Due to laser noise in the three first channels of the ASASP, those channels (ranging from 0.1 to 0.154 μm in diameter) have been excluded from this study.

The ASASP was calibrated with ammonium sulphate particles prior to the experiment. A schematic flow diagram of the calibration is shown in Fig. 3. While a complete description of the calibration is beyond the scope of this paper, details pertaining to the ASASP will be discussed here. A solution of either ammonium sulfate or a mixture of polystyrene latex spheres was atomized and then dried and diluted in a mixing chamber to produce a polydisperse aerosol. The aerosol then passed through a TSI 3071 differential mobility analyzer, where a single particle mobility was selected. The monodisperse (strictly speaking, monomobile) aerosol then passed through a plenum to the various instruments. A TSI 3020 CNC was used as a reference for determining the counting efficiency of the OPCs. In this manner, the sizing characteristics of the ASASP were determined, as well as its counting efficiency. This information was incorporated into a calibration curve for the OPC.

The calibration was done in the 0.1–1-μm diameter range. For the 1–10-μm range, the same conversion factor as below 1 μm was applied to the manufacturer's latex calibration curve to account for the difference in scattering behavior of ammonium sulphate and latex spheres. Due to Mie scattering effects, particles in the 0.5–1-μm range are not uniquely sized by laser OPC instruments. In that size range, a rebinning algorithm was applied to the data. The algorithm reduced the size resolution as compared to the manufacturer's in order to minimize sizing ambiguities.

When operating the OPC at high altitudes, the mirror at one end of the laser cavity must be adjusted to account for changes in the refractive index of air. The laser power of the OPC tended to decrease with increasing altitude. This problem was circumvented by adjusting the mirror *at altitude* so that the laser reference voltage was maximized at the sampling level.

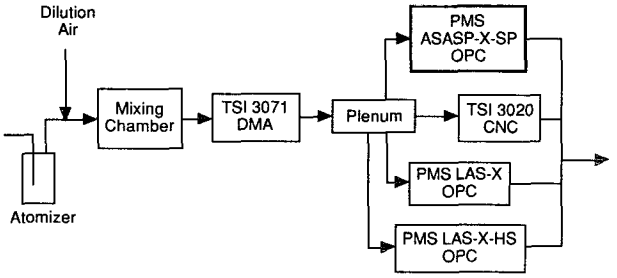

FIG. 3. Flow diagram for the ASASP calibration.

c. *CVI discussion*

The airborne version of the CVI probe has a 90° bend in the sampling line 40 cm downstream of the tip of the probe. Any cloud elements with an aerodynamic size larger than approximately 30 μm will impact on the wall in this bend with 50% efficiency (Cheng and Wang 1981). The temperature of the sample airstream in the CVI was roughly 300 K, and the relative humidity was less than 1% during this experiment. The pressure in the probe will be that of the atmosphere (plus ram pressure) at the level of sampling. Calculating the evaporation times for droplets under these conditions tells us that any droplets larger than approximately 50–60 μm will not make it around the bend. That a cloud element hits the inside wall of the probe means that the residual particle from the probe will be lost but the water from the cloud element will still be given off to the sample airstream. A cloud element that has passed the bend without impacting still has roughly 2 m to go before reaching the plenum to which the sampling instruments are connected. The evaporation time of a 60-μm-diameter droplet, for example, at a pressure of 400 hPa in the probe is less than 500 ms. Ice crystals ending up in the CVI will evaporate and melt at the same time. An ice crystal with a shape of a 60-μm sphere will probably have a slightly longer lifetime in the CVI than that of a cloud droplet of the same size, but ice crystals usually have shapes with higher surface-to-volume ratios than that of spheres, which will shorten the evaporation time. Since the total residence time of a cloud element in the CVI system before reaching the plenum is on the order of 2.5 s, all cloud elements should have evaporated before they reach the instruments.

The sampling rate of the data acquisition system was 1 Hz. Due to the different response times of the instruments, an averaging time of 30 s has been applied to the data.

3. Experimental results

Data from five cirrus flights will be presented here. One of the flights was done in prefrontal cirrus uncinus and floccus clouds. The remaining flights took place on four consecutive days in cirrostratus clouds. Since these four days were quite similar, they will be treated together.

For all measurements, the values presented have been reduced to standard temperature and pressure (STP; 0°C, 1 atm).

a. Cirrus uncinus and floccus

On 20 September 1989 a strong upper-level trough was situated to the west of the British Isles, while the sampling area was still under the influence of a high pressure system. A frontal system lying just northeast of Great Britain had thick cirrus ahead of the warm front to the north of the working area. Bands and patches of uncinus and floccus stretched southward over the sampling area.

Figure 4 shows a time series for the CWC from both Lyman-α hygrometers and the total number concentration of cloud elements measured with the CNC and OPC. The gaps in the times series are for those times when the Lyman α was zeroed or when the CNC values could not be used due to pressure effects. Figure 4 shows

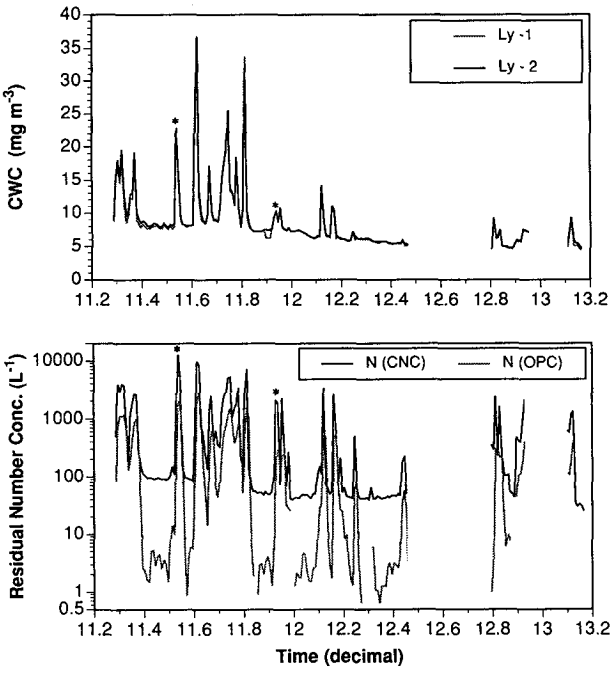

FIG. 4. Time series for 20 October. The CWC from both the 5-cm (dashed line) and the 15-cm (full line) Lyman-α hygrometers is plotted in the upper figure. The peaks marked with stars are occasions where crystal shattering may have occurred. In the lower figure, the residual number concentration measured by the CNC is plotted with a full line, and the total concentration measured by the OPC is plotted with a dashed line. The averaging time in the time series is 30 s.

the good agreement between the two Lyman-α hygrometers. The deviation between the two hygrometers was never more than 2 mg m^{-3}. The average deviation during the whole flight is 0.3 mg m^{-3}. For the number concentration data, a notable feature is that, as expected, the OPC always showed lower concentrations than the CNC. On average, for all flights, the OPC number concentrations were approximately 20% of those of the CNC. This can be explained by the difference in the lower detection limit of the two instruments.

For most of the peaks in Fig. 4, the operator was able to ascertain visually that the aircraft was inside a cloud, although for a few of the peaks this was not possible. Between the peaks, there is a "background" in both the CWC and number concentration. During these periods, the hygrometers, and the CNC and OPC, never reached zero values. This background had a CWC of 8 mg m^{-3} at the beginning of the flight and decreased to 5 mg m^{-3} toward the end of the flight. The background number concentration measured by the CNC was approximately 30–100 l^{-1}, and that by the OPC was 1–5 l^{-1}, occasionally measuring a zero concentration. Most of the time, cirrus clouds could be seen above the aircraft, both close to and high above our flight level. There were occasions, though, when no cirrus could be seen above the aircraft.

Ice crystals in clear air have been observed previously. Barnes (1980) reports on a number of measurements in what he termed "subvisible cirrus" with particle concentrations as high as 10 l^{-1}. The visibility during all of Barnes's measurements was reported to have been in excess of 100 km. On a few occasions, Barnes reported that cirrus clouds could be seen well above the aircraft. The number concentrations in these instances could be as high as 100–1000 l^{-1}. The background CWC and residual particles observed here can be interpreted as evidence of subvisible cirrus.

During the 20 September flight, sampling took place at altitudes from 7 to 8 km, with temperatures in the range of −30° to −20°C. The CWC varied from 5 to 37 mg m^{-3} during the flight, the average for the whole flight being 9 mg m^{-3}. The average cloud-element number concentration measured by the CNC was 820 l^{-1}. The OPC measured 220 l^{-1}. Calculating an average for those times that were known (through visual observation) to be in cloud, the CWC was 14 mg m^{-3}. The corresponding cloud-element number concentration was 2400 l^{-1}, as measured by the CNC while the OPC measured 630 l^{-1}. The maximum concentration measured by the CNC was 12 800 l^{-1}. The diameter of mean mass (DMM) of the cloud elements calculated from the CWC and the CNC number concentration ranged from 15 to 70 μm; the average for the whole flight was 47 μm.

b. Cirrostratus

On 15 October there was an upper-level trough over the North Sea and a warm front was situated over Great

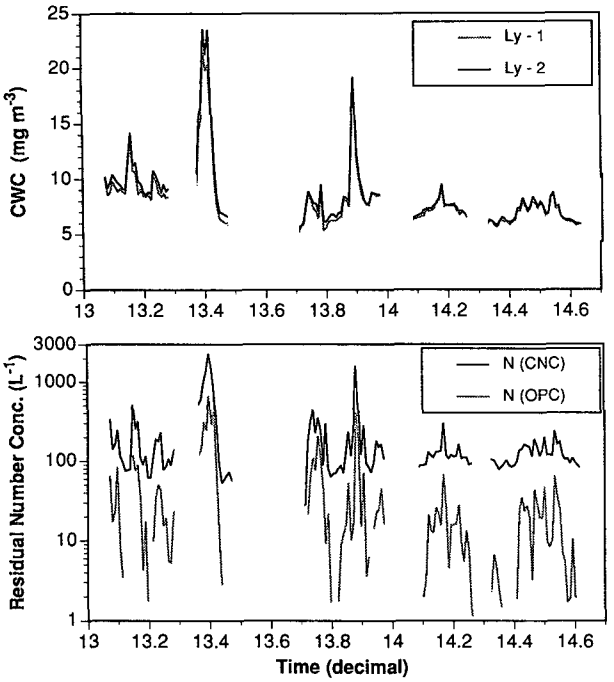

FIG. 5. The same as Fig. 1 but for 17 October.

Britain. The frontal zone and the polar jet passed the sampling area during the night of 15/16 October. During the period from 16 to 18 October, the area was under the influence of a high pressure system, and further frontal systems passed well north of the sampling area. In the warm air advected in over the area in the upper troposphere, visually thin cirrostratus formed in a layer from about 7-km altitude to at least 11.5 km (maximum altitude for the Falcon aircraft). Even though the cirrus clouds during this period were vertically thick, they were observed to be thin, and the structure of the underlying land and water could often be seen clearly through the cloud.

A time series for 17 October is shown in Fig. 5. The variables and averaging time are the same as for the uncinus and floccus case shown in Fig. 4. This time series is representative of the data for all four cirrostratus cases. The temporal development was very similar for all four days, though the absolute values varied slightly. Once again, there was good agreement between the two hygrometers. This was the case for all of the 15–18 October flights. The average deviation between the hygrometers over all four days was 0.45 mg m^{-3}, the maximum deviation being 3 mg m^{-3}.

The structure of the cirrostratus clouds was such that we seemed, most of the time, to be flying between two cloud layers. We could see cirrus above and below the aircraft, but it was very difficult to decide if there were any crystals at our flight level. The CVI showed crystals at all levels and locations in the measurement area. Neither the condensed water content nor the number concentration of cloud elements ever reached zero. The lowest concentrations were measured on 15 October. The minimum measured CWC was 1 mg m^{-3}, and the corresponding cloud-element concentration measured by the CNC was 20 l^{-1}. No residual particles larger than 0.15 μm in diameter were registered at these times.

During the four cirrostratus flights, we sampled at altitudes from 7 to 11.3 km. Even though the highest altitude flown on 15 October was 10.1 km, thin cirrus were still observed above the aircraft. The base of the cirrostratus clouds increased steadily from 7 km on 15 October to just above 9 km on 18 October. The temperatures in the cloud layers of the four days ranged from −28° to −61°C.

Table 1 contains a summary of the data for these four flights. The highest condensed water content was measured on 16 October, with a flight average of 11 mg m^{-3} and a maximum of 21 mg m^{-3}. With an average of 5 mg m^{-3}, 15 October had the lowest CWC of the four days. The highest cloud-element concentrations, with roughly 190 l^{-1}, occurred on 15 and 17 October, and a maximum concentration of 2290 l^{-1} was measured on 17 October. The cloud element concentration was lowest on 18 October, with a flight average of 80 l^{-1}. The OPC total concentration showed the same structure as the CNC. Due to the difference in the lower detection limit, the OPC concentration was on average only 20% of the CNC concentration. The diameter of mean mass (DMM) of the cloud elements increased from 47 μm on 15 October to 59 mm on 18 October. The variation in DMM during a single flight could be from approximately 23 to almost 80 μm.

c. *Size distribution of residual particles*

During all flights, measurements were made of the size distribution of residual particles from cirrus cloud elements. The number size distributions plotted in Fig. 6 are examples of number size distributions measured in cloud on 20 September. The size distributions are plotted as $dN/d\log D$, where N is the number concentration and D is the particle diameter. The shape of the plotted size distributions is characteristic for most residual size distributions, where the total concentration in the OPC is larger than 100 particles per liter. The main features of the residual number size distributions are the large peak in the size range of 0.3–0.7 μm in diameter, and the tail in the size range 1–10 μm. As the particle concentration decreased, the large particles disappeared first, and with an OPC total particle concentration less than 10 l^{-1}, there were usually only particles smaller than a few hundred nanometers measurable. Taking the difference between the CNC and the OPC total concentrations, we can construct an extra "channel" in the size distribution covering 0.02–0.15 μm in diameter. This extra channel is not plotted in Fig. 6, but it will contain around 80% of the integral

TABLE 1. Properties of the studied cirrus clouds. Designation WF denotes whole flight and VCE denotes visual cloud event.

Date	20 September		15 October	16 October	17 October	18 October
Comment	WF	VCE	WF	WF	WF	WF
Cirrus altitude (km)	6.4–7.9		7–10.1	7.6–11.3[a]	8.2–11.3[a]	9.3–11.3[a]
Temperature (°C)	−28 to −15		−52 to −28	−61 to −32	−60 to −37	−61 to −46
CWC (mg m^{-3})[b]						
Average	9	14	5	11	8	7
Range	4–36		1–18	2–21	5–22	3–11
CNC number concentration (l^{-1})						
Average	820	2400	190	160	190	80
Range	20–12 800		20–960	20–330	30–2290	30–320
OPC number concentration (l^{-1})						
Average	225	630	40	30	40	110
Range	0–2900		0–280	0–230	0–660	0–110
Diameter of mean mass (μm)[c]						
Average	47	29	47	53	52	59
Range	15–70		23–77	38–72	26–76	35–77

[a] Maximum altitude of aircraft
[b] Average of the two hygrometers
[c] Calculated from CWC and CNC values

number concentration from 0.02 to 10 μm. For distributions where the OPC concentration was higher than 100 l^{-1}, this size interval would contain typically 10^3–10^4 l^{-1}. For the times between visual cloud events, when the OPC concentration is less than 10 l^{-1}, this size interval contained roughly 10–100 l^{-1}.

It is uncertain if the double peak in the 0.3–0.7-μm range is real or an instrument artifact. There is a consistent local minimum at about 0.5 μm. At the wavelength of the laser used in this OPC, the intensity of the light scattered by particles in this size range is not a single-valued function of particle size. This minimum has also been observed in residual size distributions from radiation fog droplets in a later experiment. While the rebinning algorithm applied to the OPC data was intended to minimize these Mie scattering effects, it is not clear at this time whether this local minimum is significant.

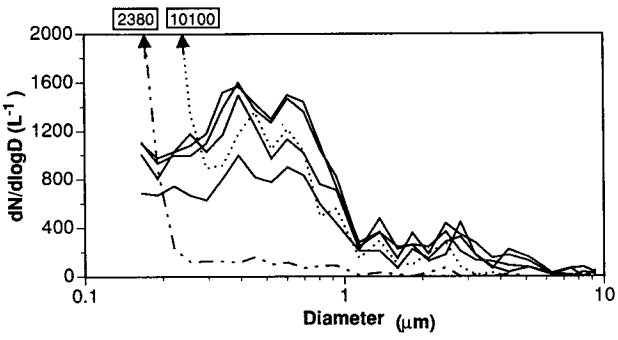

FIG. 6. Size distributions of residual particles detected by the OPC on 20 October. Total concentrations for these size distributions are 300–1900 l^{-1}. The averaging time for each size distribution is 30 s. The counting error for a total particle concentration of 700 l^{-1} sampled over 30 s is approximately 20%.

4. Discussion

For most of the flights, the cloud-element number concentrations and condensed water contents are in the range of previously reported values. Dowling and Radke (1990) have summarized a large fraction of the existing literature on cirrus clouds. The ranges of the measurements compiled by Dowling and Radke are 10^{-4}–1.2 g m^{-3} for the ice water content and 10^{-4}–10^4 l^{-1} for the crystal number concentration. With condensed water contents in the range 1–36 mg m^{-3} and number concentrations from 10 to 12 800 l^{-1}, the measurements reported here are in the range of those included in the Dowling and Radke survey. Our data tend to be at the low end of the ice water content range, while simultaneously at the high end of the number concentration range.

Due to the high number concentrations on 20 September, there was some concern as to whether these concentrations were real or were due to shattering of the crystals in the CVI probe. Only Ryan et al. (1972) and Platt et al. (1989) have measured concentrations as high as 10^4 l^{-1} in cirrus clouds. Their measurements were performed with instruments designed for studies of spherical droplets (and not ice crystals); these instruments can have large errors in the measured number concentrations.

Since cloud elements are rapidly decelerated in the CVI, it may be possible for some of them to develop wakes as they slow down. A potential problem that arises in this case is that small particles may be entrained in the wakes and appear in the sample stream.

Typical concentrations of particles larger than approximately 0.02 μm in diameter are between 0.02 and 5 l^{-1} (Junge 1961; Hofmann and Rosen 1985; Hofmann et al. 1990). For all of the data discussed here, the CVI was operated at its lowest cut size. Under these conditions, the stagnation plane inside the probe is located close to the probe tip. At the point that cloud elements could develop wakes, there would have been no interstitial particles (or residual particles from very small cloud elements) present to be entrained. At higher cut sizes, the potential for wake entrainment may be larger; however, at the low cut sizes we discuss here, we estimate that the effects of wake entrainment would have been negligible.

The initial Reynolds number for a particle having the observed average diameter of mean mass (discussed below) of 50 μm and an initial velocity of 200 m s^{-1} would have been approximately 250. This is well outside the Stoke's flow regime, indicating that crystal shattering may have been a problem.

We examined crystal shattering using the measurements of the size distribution of the residual particles. With the possible exception of two peaks in the time series shown in Fig. 4 (flagged with asterisks), we are reasonably certain that the large number of concentrations we observed were not due to ice-crystal shattering. Figure 6 shows examples of residual size distributions measured by the OPC on 20 September. If there was shattering of crystals, we would expect to see a shift in the number concentrations from larger to smaller sizes. This can be seen only on two occasions during this day: for the peak with the highest number concentration (12 800 l^{-1} as measured by the CNC), and for the first of the double peaks at roughly 11.9 h (approximately 2000 l^{-1} by the CNC). The size distributions corresponding to these occasions are plotted in the figure as the dotted and dash–dot lines, respectively. These two curves show the expected shift to smaller sizes if there is crystal shattering.

Examining the difference between the CNC and the OPC total concentrations ($N_{CNC} - N_{OPC}$) as a function of the CNC concentration should also reveal whether there was any splintering that resulted in residual particles smaller than 0.15 mm in diameter. Our results (not shown here) indicate that there is no increase in the difference as the total residual particle concentration increases, as would be expected if there was splintering of particles. Although the above arguments do not prove that the crystal shattering did not cause the high number concentrations, they do indicate that the observations were real.

Another potential cause for the large numbers of residual particles could be that the residual particles themselves shattered, as opposed to the ice-crystal shattering discussed above. Laboratory investigations of the CVI by Anderson (1992) indicate, however, that, for the CVI, the shattering of cloud elements is the major process by which artificially high concentrations of small particles can be produced. In either case, the end effect is the same and can be detected using the technique described above.

In Dowling and Radke (1990) (hereafter referred to as DR), eight of the cited papers reported cirrus cloud measurements with a lower detection limit in the range of 1.5–5 μm, in most cases corresponding to the FSSP detection limit. In three of these [Heymsfield 1977; Heymsfield et al. 1990 (in DR referenced as Miller et al. 1990); Sassen et al. 1989] the FSSP measurements are not included in the reported concentration values. Since most of the measurements reported in DR are for crystals larger than 20 μm, while our measurements are for crystals with a Stokes diameter down to 4 μm, it is perhaps not surprising that our measurements are in the upper range of the reported number concentrations.

While we do not directly measure the sizes of the cloud elements, we can obtain a frequency distribution of the time-averaged diameters of mean mass. The DMM is calculated from the measured liquid water content and particle number. Such distributions are shown in Fig. 7 for two flights. These are histograms of the percentage of the total number of 30-s averaging intervals during each flight in which a given DMM was measured. For the cirrostratus case from 15 October, the distribution of DMM values is slightly asymmetrical, centered around the average of 47 μm. The range of the cloud-element number concentration was 20–

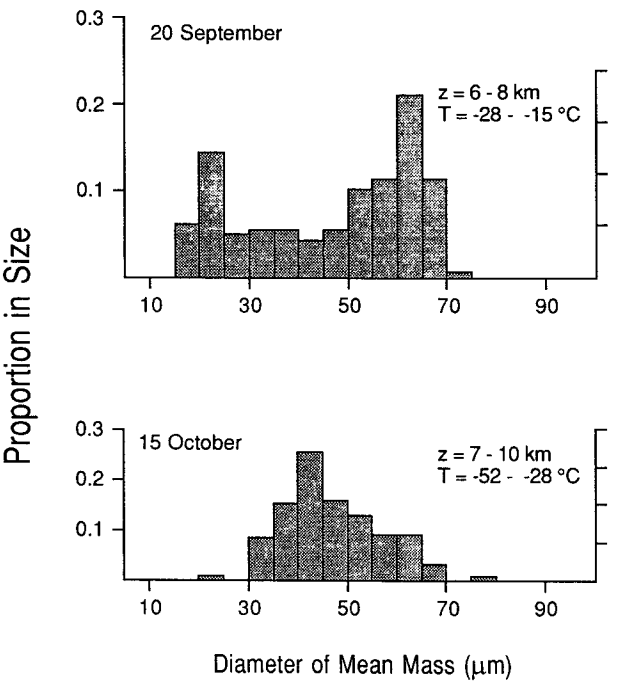

FIG. 7. Diameter of mean mass histograms. The percentages of the total number of 30-s intervals, when a given DMM value was observed, is plotted. Flights from 20 September and 15 October are shown.

960 l^{-1}. There were no instances of the very high concentrations observed on 20 September. The histogram in Fig. 4 for flight 202 shows two modes; one at approximately 20 μm and the other at approximately 60 μm. The average DMM for the whole of flight 202 is 47 μm—the same as for the flight on 15 October. However, if we average only those instances when the observer was able to confirm visually that the aircraft was in cloud, the average DMM for this flight is 29 μm.

It appears that there may have been two populations of cloud elements in these uncinus–floccus clouds. In the visually thick clouds, the cloud elements were small and had large number concentrations. Between the visually detectable clouds, there were larger cloud elements, with lower number concentrations. This can also be seen by plotting the DMM versus the cloud-element number concentration. These plots for the two flights are shown in Fig. 8. The plot for the 20 September case shows that the smallest crystals had the largest number concentrations. There were a substantial number of averaging intervals that gave DMM values between 20 and 30 μm. Most of these instances were associated with number concentration values greater than 1000 l^{-1}. For the flight on 15 October, there was only a single DMM value below 30 μm, and there were no instances of number concentrations greater than 1000 l^{-1}.

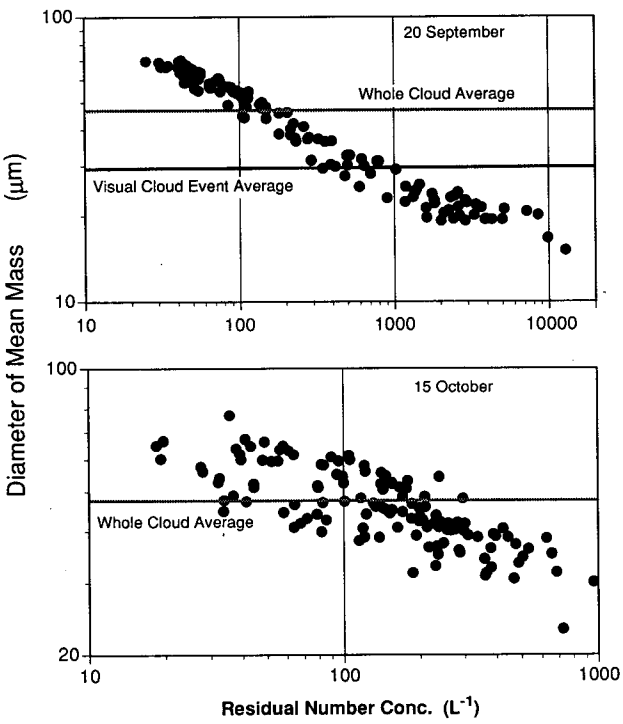

FIG. 8. DMM versus cloud-element number concentrations. Two flights are shown: 20 September and 15 October. The 20 September flight shows instances of small cloud elements with large number concentrations.

Considering the large number concentrations measured and the fact that the DMM is calculated from a "bulk" condensed water content, DMM values of 20–30 μm means that there must have been large numbers of crystals (or droplets) smaller than these radii present in the cloud. These small crystals will be important for the radiative properties of the cloud. The number of crystals (or droplets) smaller than roughly 20 μm could have been quantified by increasing the cut size of the CVI and then comparing the measurements with those where the cut size was at the smallest cut size (4 μm). Since our main objective during ICE '89 was to determine the total condensed water content, this change in cut size was never done.

5. Summary and conclusions

We have presented cloud microphysical properties for one cirrus uncinus–floccus case, and four cirrostratus cases during the ICE '89 experiment. Direct measurements of the condensed water content were made using the counterflow virtual impactor. Measurements of the number concentration and size distribution of the residual aerosol particles released by evaporated cloud elements were also made.

In the cirrus uncinus and floccus case, sampling took place at altitudes from 7 to 8 km, and with temperatures ranging from −20° to −30°C. The average CWC for the visually detectable clouds was 14 mg m^{-3}, and the number concentration was 2400 l^{-1}. The diameter of mean mass for the cloud elements in these cases was 29 μm.

For the cirrostratus cases (four consecutive days), the cloud base increased from 7 km on the first day to 9 km on the last day. There were clouds present at altitudes higher than the maximum of the aircraft, 11.3 km. The average cloud-element number concentration ranged from 85 to 190 l^{-1} over the four days. The average CWC for the four days ranged from 5 to 11 mg m^{-3} over the four days. The average diameter of mean mass of the cloud elements ranged from 37 to 54 μm.

In cirrus uncinus–floccus clouds, we observed cloud-element diameters of mean mass that were lower than what the most commonly used crystal sizing instruments can detect. Due to the relatively high temperatures in these clouds, it is possible that these cloud elements could have been liquid droplets. In the cirrostratus cases, the cloud elements were likely to be ice crystals. Whatever their phase or crystal habit, these small crystals will be important in determining the radiative properties of the clouds.

The residual number size distributions from the cloud elements exhibited a broad peak in the 0.3–0.7-μm diameter range, with a tail in the 1–10-μm range. In terms of number, most of the residual particles were in the 0.02–0.15-μm range.

We have demonstrated that the CVI can be used to

examine several important characteristics of cirrus clouds. It is a useful tool for obtaining information about the smaller cirrus cloud elements, their number, and condensed water content. It is also useful in obtaining information about the aerosol that was scavenged by the cloud elements. As examples, future experiments could focus on 1) obtaining a total water (vapor and condensed-phase) budget for cirrus clouds to better determine their radiative properties, 2) determining the scavenging efficiency for the aerosol in cirrus clouds to better understand the life cycles of cirrus clouds, and 3) determining the chemical composition of the scavenged and nonscavenged aerosol in cirrus to better understand cirrus formation.

Acknowledgments. We would like to thank Leif Bäcklin, Sven-Åke Odh, and Sune Moritz for their help with the CVI payload. André Zuber was very helpful in the work with the Lyman-α hygrometers. The DLR personnel, especially the pilots and crew of the *Falcon,* were indispensable. We are indebted to Keith Bigg for his help in interpreting the data.

REFERENCES

Anderson, T. L., 1992: Optimization of a counterflow virtual impactor (CVI) for studying aerosol effects on cloud droplet number. PhD thesis, University of Washington, 232 pp.

Barnes, A. A., Jr., 1980: Observations of ice particles in clear air. *J. Rech. Atmos.,* **14,** 311–315.

Cheng, Y. S., and C. S. Wang, 1981: Motion of particles in bends of circular pipes. *Atmos. Environ.,* **15,** 301–306.

Dowling, D. R., and L. F. Radke, 1990: A summary of the physical properties of cirrus clouds. *J. Appl. Meteor.,* **29,** 970–978.

Gardiner, B. A., and J. Hallett, 1985: Degradation of in-cloud forward scattering spectrometer probe measurements in the presence of ice particles. *J. Atmos. Oceanic Technol.,* **2,** 171–180.

Heintzenberg, J., J. A. Ogren, K. J. Noone, and L. Gärdneus, 1989: The size distribution of submicrometer particles within and about stratocumulus cloud droplets on Mt. Åreskutan, Sweden. *Atmos. Res.,* **24,** 89–101.

Heymsfield, A. J., 1975: Cirrus uncinus generating cells and the evolution of cirriform clouds. Part I: Aircraft observations of the growth of the ice phase. *J. Atmos. Sci.,* **32,** 799–808.

——, 1977: Precipitation development in stratiform ice clouds: A microphysical and dynamical study. *J. Atmos. Sci.,* **34,** 367–381.

——, 1986: Ice particles observed in a cirriform cloud at −83°C and implications for polar stratospheric clouds. *J. Atmos. Sci.,* **43,** 851–855.

——, and R. G. Knollenberg, 1972: Properties of cirrus generating cells. *J. Atmos. Sci.,* **29,** 1358–1366.

——, and C. M. R. Platt, 1984: A parameterization of the particle size spectrum of the ice clouds in terms of the ambient temperature and the ice water content. *J. Atmos. Sci.,* **41,** 846–855.

——, and L. M. Miloshevich, 1989:.Evaluation of liquid water measuring instruments in cold clouds sampled during FIRE. *J. Atmos. Oceanic Technol.,* **6,** 378–388.

——, K. M. Miller, and J. D. Spinhirne, 1990: The 27–28 October 1986 FIRE IFO cirrus case study: Cloud microstructure. *J. Atmos. Sci.,* **118,** 2314–2328.

Hofmann, D. J., and J. M. Rosen, 1985: Delayed production of sulfuric acid condensation nuclei in the polar stratosphere from El Chichon volcanic vapors. *J. Geophys. Res.,* **90,** 2341–2354.

——, T. Deshler, F. Arnold, and H. Schlager, 1990: Balloon observations of nitric acid aerosol formation in the arctic stratosphere: II. Aerosol. *Geophys. Res. Lett.,* **17,** 1279–1282.

Junge, C. E., 1961: Vertical profiles of condensation nuclei in the stratosphere. *J. Meteor.,* **18,** 501–509.

Noone, K. J., and H.-C. Hansson, 1990: Calibration of the TSI 3760 condensation nucleus counter for nonstandard operating conditions. *Aerosol Sci. Tech.,* **13,** 478–485.

——, J. A. Ogren, J. Heintzenberg, R. J. Charlson, and D. S. Covert, 1988a: Design and calibration of a counterflow virtual impactor for sampling of atmospheric fog and cloud droplets. *Aerosol Sci. Tech.,* **8,** 235–244.

——, R. J. Charlson, D. S. Covert, J. A. Ogren, and J. Heintzenberg, 1988b: Cloud droplets: Solute concentration is size dependent. *J. Geophys. Res.* **93D,** 9477–9482.

——, J. A. Ogren, A. Hallberg, J. Heintzenberg, J. Ström, H. C. Hansson, B. Svenningsson, A. Wiedensohler, S. Fuzzi, M. C. Facchini, B. G. Arends, and A. Berner, 1992: Changes in aerosol size and phase distributions due to physical and chemical processes in fog. *Tellus,* **44B,** 489–504.

Ogren, J. A., J. Heintzenberg, and R. J. Charlson, 1985: In-situ sampling of clouds with a droplet to aerosol converter. *Geophys. Res. Lett.,* **12,** 121–124.

——, ——, A. Zuber, K. J. Noone, and R. J. Charlson, 1988: Measurements of the size-dependence of non-volatile aqueous mass concentrations in cloud droplets. *Tellus,* **41B,** 24–31.

——, K. J. Noone, A. Hallberg, J. Heintzenberg, D. Schell, A. Berner, I. Solly, C. Kruisz, G. Reischl, B. G. Arends, and W. Wobrock, 1992: Measurements of the size dependence of the concentration of non-volatile material in fog droplets. *Tellus,* **44B,** 570–580.

Platt, C. M. R., J. D. Spinhirne, and W. D. Hart, 1989: Optical and microphysical properties of a cold cirrus cloud: Evidence for regions of small particles. *J. Geophys. Res.,* **94,** 11 151–11 164.

Ryan, R. T., H. H. Blau, P. C. von Thüna, M. L. Cohen, and G. D. Roberts, 1972: Cloud microstructure as determined by an optical cloud particle spectrometer. *J. Appl. Meteor.,* **11,** 149–156.

Sassen, K., D. O'C. Starr, and T. Uttal, 1989: Mesoscale and microscale structure of cirrus clouds: Three case studies. *J. Atmos. Sci.,* **46,** 371–396.

Stephens, G. L., S.-C. Tsay, P. W. Stackhouse, Jr., and P. J. Flatau, 1990: The relevance of the microphysical and radiative properties of cirrus clouds to climate and climatic feedback. *J. Atmos. Sci.,* **47,** 1742–1753.

Twohy, C. H., A. D. Clarke, S. G. Warren, L. F. Radke, and R. J. Charlson, 1989: Light-absorbing material extracted from cloud droplets and its effect on cloud albedo. *J. Geophys. Res.,* **94,** 8623–8631.

Zuber, A., 1989: Resonant light sources and their use in atmospheric research. Ph.D. dissertation, Stockholm University, Stockholm, Sweden, 300 pp.

——, and G. Witt, 1987: Optical hygrometer using differential absorption of hydrogen lyman-a radiation. *Appl. Opt.,* **26,** 3083–3089.